



HAL
open science

The impact of curved-tip propeller geometry on hovering drone performance for air quality monitoring

Mohamed Abdessamia Chakchouk, Abdelkhalak El Hami, Pierre Richard Dahoo, Azzedine Lakhlifi, Wajih Gafsi, Mohamed Haddar

► To cite this version:

Mohamed Abdessamia Chakchouk, Abdelkhalak El Hami, Pierre Richard Dahoo, Azzedine Lakhlifi, Wajih Gafsi, et al.. The impact of curved-tip propeller geometry on hovering drone performance for air quality monitoring. *Advances in Mechanical Engineering*, 2023, 15 (10), 10.1177/16878132231206330 . hal-04271271

HAL Id: hal-04271271

<https://hal.science/hal-04271271>

Submitted on 27 May 2024


HAL is a multi-disciplinary open access archive for the deposit and dissemination of scientific research documents, whether they are published or not. The documents may come from teaching and research institutions in France or abroad, or from public or private research centers.

L'archive ouverte pluridisciplinaire **HAL**, est destinée au dépôt et à la diffusion de documents scientifiques de niveau recherche, publiés ou non, émanant des établissements d'enseignement et de recherche français ou étrangers, des laboratoires publics ou privés.



Distributed under a Creative Commons Attribution 4.0 International License

The impact of curved-tip propeller geometry on hovering drone performance for air quality monitoring

Advances in Mechanical Engineering
2023, Vol. 15(10) 1–11
© The Author(s) 2023
DOI: 10.1177/16878132231206330
journals.sagepub.com/home/ade


Mohamed Abdessamia Chakchouk¹ , Abdelkhalak El Hami²,
Pierre Richard Dahoo³, Azzedine Lakhlifi⁴, Wajih Gafsi¹
and Mohamed Haddar¹

Abstract

The success or failure of a drone mission depend on several elements, including the drone's mass and payload, the surrounding environment, the battery's state, and the propulsion system's performance. Several studies have been undertaken addressing the propeller performance of this final component, particularly for fixed-wing or quad copter drones with ducted propellers. However, the shape of propeller blades used on tiny civil drones has not drawn as much attention. In this research work, the performance characteristics of a 10 × 4.7-inch curved tip propeller were explored, with the Advanced Precision Composite drone propeller serving as a design reference. This study seeks an alternative to ducted propellers when mass or size limitations prevent their use. The Computational Fluid Dynamics model was confirmed by comparing simulation results to the experimental propeller data source established by the University of Illinois at Urbana-Champaign, starting with a standard type propeller and using thrust coefficient as the key performance indicator. Moreover, the data analysis for the bended tip propeller replicating the well-established model, revealed the benefits as well as the drawbacks of such propellers on the mission profile and the battery lifespan of a quad copter Unmanned Air Vehicle.

Keywords

Propeller blades, propeller performance, unmanned air vehicle, computational fluid dynamics analysis, surrogate model, battery lifetime

Date received: 29 August 2023; accepted: 4 September 2023

Handling Editor: Chenhui Liang

Introduction

The performance of drones is significantly influenced by the design and operation of their propellers, which impact crucial parameters such as efficiency, stability, maneuverability, and flight duration.^{1,2} The aerodynamics of propellers, particularly the generation and management of propeller vortices, play a vital role in defining flight performance.³ However, these vortices can lead to reduced thrust, increased noise, equipment interference, and potential threats to the propulsion system's integrity.^{4,5}

To enhance propeller performance, numerous strategies have been explored, including the use of ducts to

¹Ecole Nationale des Ingénieurs de Sfax, Sfax, Tunisie

²INSA de Rouen, Saint Etienne de Rouvray, Rouen, France

³Université ParisSaclay, UVSQ, CNRS, Guyancourt, Versailles, France

⁴Université de Franche-Comté, Besançon, France

Corresponding author:

Mohamed Abdessamia Chakchouk, Ecole Nationale des Ingénieurs de Sfax, Route de sokra, KM 4, Sfax 3038, Tunisie.

Email: mohamed-abdesamii.chakchouk@enis.tn



Creative Commons CC BY: This article is distributed under the terms of the Creative Commons Attribution 4.0 License (<https://creativecommons.org/licenses/by/4.0/>) which permits any use, reproduction and distribution of the work

without further permission provided the original work is attributed as specified on the SAGE and Open Access pages (<https://us.sagepub.com/en-us/nam/open-access-at-sage>).

mitigate propeller noise. However, this approach has inherent constraints.⁶

Insightful numerical investigations by Mi⁷ have highlighted the significant influence of environmental factors, such as ground, sea surface, and wave conditions, on the aerodynamic properties of ducted propellers. Extensive research efforts have focused on optimizing ducted fan efficiency and stability through flow control techniques and innovative configurations.⁸ This emphasizes the critical interplay between propeller design and external environmental conditions.

Comparative studies have been conducted to assess the aerodynamic performance of contra-rotating ducted fans and open contra-rotating fans researchers, such as Akturk and Camci,^{9,10} have provided valuable insights into the complex flow field dynamics during hovering and crosswind operations. Chen et al.¹¹ have emphasized the need for further innovation in ducted propeller design, particularly for hovering tasks. Their inventive design incorporating a tip jet for VTOL aircraft has demonstrated enhanced blade thrust, albeit with an increased overall weight.

The use of ducted propellers in high-speed forward flight presents challenges due to increased drag.¹¹ Pitching moment and architectural constraints affect their stability and overall system efficiency.¹² Proximity effects, such as ground effect, can induce rotational stall phenomena and reduce flow rate.¹³ Tip clearance and the number of blades in a propeller are additional design considerations that impact performance.^{14–24} The use of ducts is then limited in certain circumstances, researchers aim in this case to improve the performance of the propeller system otherwise. Optimizing propeller shape, including chord length, pitch angle, twist, sweep, and lean, is crucial for efficient and high-performance propellers.^{25–31} Studies have demonstrated the impact of these design elements on propeller efficiency, pressure ratio, and structural performance.²⁸ Spiroid winglets have shown potential in reducing wingtip vortices and improving aircraft efficiency.^{32–34} High aspect ratio wings have been favored for their reduced induced drag.³⁵

To fill this research gap, our study conducts a groundbreaking investigation into the performance of a 10×4.7 -inch propeller with curved tips, a design inspired by the marine industry's Kappel propeller and modeled after the widely used APC drone propeller. This propeller design has not been thoroughly investigated within the context of drone applications. The implications of the modified shape on the overall drone performance are then examined. By scrutinizing the aerodynamic performance of the bended tip propeller, this study aspires to enrich the collective understanding of propeller design for drones, thereby laying the groundwork for further advancements in this domain.

Background

To determine lift and torque of a propeller, the simple blade element theory suggests calculating the aimed physical quantities for each of these elements and then summing them. This theory demonstrates the significance of each element in the propeller's geometry as a fundamental aspect of its efficiency.³⁷ Since the propeller blade will be set at a given geometric pitch angle (β), the local velocity vector will create a flow angle of attack on the section. In this respect lift and drag components normal to and parallel to the propeller disk can be calculated so that the contribution to thrust and torque of the complete propeller from this single element can be obtained.³⁷

The difference in angle between thrust and lift directions is defined as:

$$\phi = \beta - \alpha \quad (1)$$

The elemental thrust and torque of this blade element can thus be expressed in terms of:

$$\Delta T = \Delta L \cos(\phi) - \Delta D \sin(\phi) \quad (2)$$

$$\frac{\Delta Q}{r} = \Delta D \cos(\phi) + \Delta L \sin(\phi) \quad (3)$$

The operation of a propeller can be handled using the same physical principles as that of a wing. The propeller has air moving around the top and bottom, creating a high-pressure zone and a low-pressure zone.

The most common practice to enhance propeller performance is adding ducts, as portrayed in Figure 1. However, ducted propellers pose additional challenges for a drone, as good efficiency necessitates very small clearances between the blade tips and the duct. Its weight increases the overall weight of the drone and at high angles of attack, parts of the duct will stall and produce aerodynamic drag. Unless these problems are solved, the duct loses its main purpose and becomes unbeneficial to install. In fact, the more parts are added to a rotational structure, the more uncertainties are created. For this reason, racing drones do not rely on using ducts, which is the case for the special drone mission like "Ingenuity" that NASA sent to mars.

To find a descent substitute to the ducted propeller, the curved tip propeller will be discussed in this paper, as recorded in Figure 2. It corresponds to a promising technology that is utilized in the maritime area.^{39–42} To some extent, the higher the bend angle is, the greater the reduction in propeller drag.⁴¹ Curved-Tip propellers, as opposed to ducted, tandem, or contra-rotating propellers, may respond suitably to these requirements. A simple technique to enhance propulsive efficiency is to shift the span wise load distribution toward the propeller tip. The Kappel propellers, used in the maritime transport field, adopt a similar approach. In this

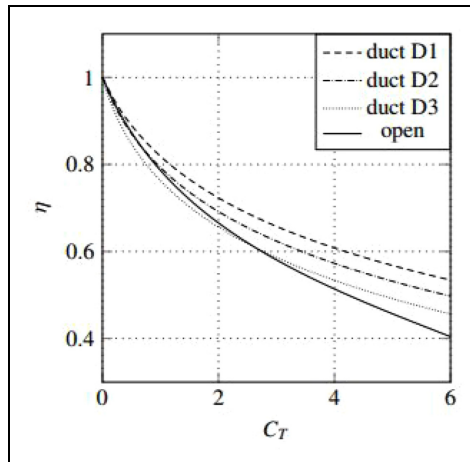


Figure 1. Ducted propeller and free propeller performance.³⁸

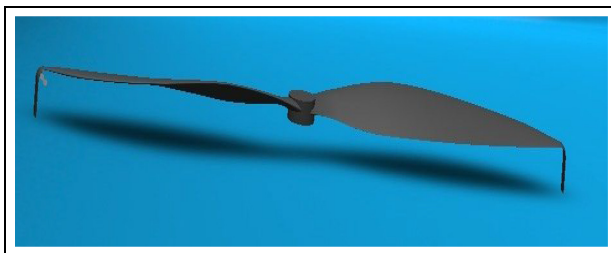


Figure 2. Curved tip propeller.

case,^{43–45} the “endplate” is a continuous piece of the blade rather than an extra foil at the tip, and it effectively points toward the suction side (as with aircraft winglets).

Methodology

The starting point for our analysis was the selection of the conventional APC slow flyer propeller, specifically the 10×4.7 -inch variant. This propeller served as a benchmark for comparison and provided a reference point for evaluating the performance of the modified design. To determine the appropriate motors for our study, we utilized a surrogate model developed with SCILAB. The surrogate model was crucial in modeling the flight plan and ensuring drone stability. From the stability analysis viewpoint described in our previous work,^{46,47} we derived the range of rotational speeds that the propellers could achieve. By analyzing the data, for each suggested propeller type we identified the propeller with the RPM range best supported by the chosen motors. The CFD analysis model was established in two stages. Firstly, using the conventional APC propeller, we selected the thrust coefficient as the primary performance criterion to validate the

numerical setup accuracy by comparing the results with those found in Illinois database.³⁶ This step allowed us to ensure the reliability and consistency of our CFD performed using ANSYS Fluent 20 R1.

In the second part of the study, we optimized the propeller design by curving the tips by 90° , using SOLIDWORKS software to help reduce vortices. To assess the performance of the modified propeller design, we replicated the validated CFD analysis using the same parameters, but with the modified propeller design. We focused on evaluating the propeller’s aerodynamic performance and its impact on the flight time duration and the maximum payload capacity. This was done by coupling the Ansys fluent simulation data to a developed MATLAB algorithm that calculate these quantities based on the given equation listed in the end of the discussion.

Numerical setup

Flow domain

Before starting the simulation, the stationary domain’s inlet, outlet, and boundary were stretched to guarantee that the flow is completely developed as it enters and departs from the simulation domain. The intake boundary was eight times the diameter D from the propeller’s origin and the outlet boundary. The enclosure was set, as foregrounded in Figure 3, to $1.1D$ for the rotating domain and to $0.4D$ for the stationary and rotating domains, respectively.

Mesh generation

The flow field of the propeller was stationary in the rotating coordinate system. The ANSYS FLUENT CFD physics preference was used to settle the problem. To discretize the governing equations, the finite volume method with a pressure-based solver was applied. The grid was fully tetrahedral in both the rotating and static zones, as depicted in Figure 4. Tetrahedral elements fitted arbitrary shaped geometries very well with their simple computations so as to reduce the cost of computation.

Engineers frequently aim for 15–30 inflation layers ($N = 15$ to $N = 30$) through the thickness of the boundary layer when creating the mesh for turbulence modeling. Turbulence modeling for aerodynamic flows using Reynolds-averaged Navier-Stokes (RANS) was carried out on a single sheet of material rather than numerous layers, as illustrated in the instance above.⁴⁸

$$\text{Re} = \frac{\rho UL}{\mu} \quad (4)$$

The Reynolds number gives a measure of the ratio of inertial forces to viscous forces and can be used to

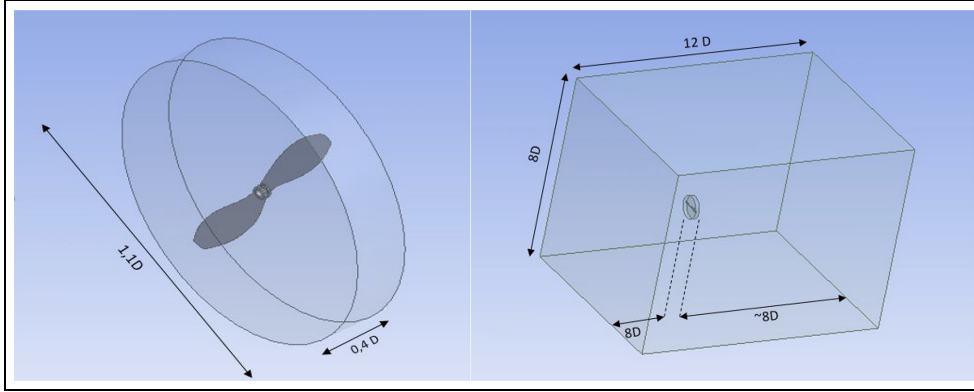


Figure 3. Flow domains.

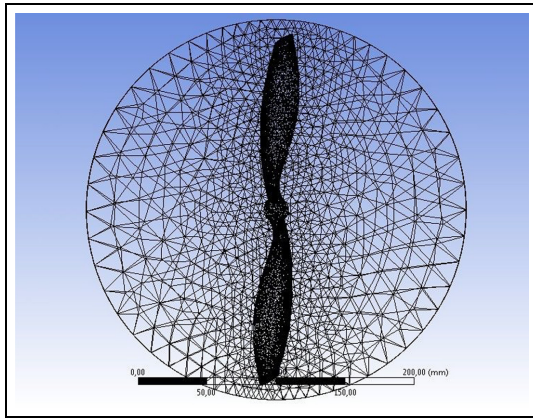


Figure 4. Generated mesh.

Table 1. Mesh quality parameters.

| Mesh metric | Minimal value | Maximal value | Average |
|-----------------|---------------|---------------|---------|
| Element quality | 5.402e-002 | 1 | 0.82935 |
| Skewness | 8.605e-006 | 0.97 | 0.24 |
| Aspect ratio | 1.1594 | 31.06 | 1.8701 |

determine if a flow will be laminar or turbulent, where ρ is the fluid density, U is the freestream velocity, L is the geometry's characteristic length, and μ dynamic viscosity of the fluid. The skin friction coefficient was then estimated using an equation that specifies out how much friction there is on a given surface.³⁷

$$C_f = [2 \log_{10}(\text{Re}) - 0.65]^{-2.3} \quad (5)$$

After calculating the skin friction coefficient, the wall shear stress (w) was determined in terms of

$$\tau_w = 0.5 * \rho U^2 C_f \quad (6)$$

The y^+ equation can be tweaked to get the height of the wall next cell centroid from the wall (y_p), yielding

y_h . The cell's height y_h is twice the value of y_p , and the distance between the cell centroid and the wall is y_p ⁴⁹;

$$y^+ = \frac{\rho y_p u_t}{\mu} \quad (7)$$

$$y_h = 2y_p \quad (8)$$

As the skin friction coefficient was calculated empirically for each flow situation, the starting cell height provided by these equations provided only an approximation. In real-world CFD calculations, skin friction coefficients are anticipated to be comparable, but not identical, to those of a flat plate. Resting on this calculation, the element size criteria were imposed as $3e-3$ on the surface of the propeller. An adaptive sizing was implemented on the stationary domain and the growth rate was fixed at 20%. The inflation was set to be program controlled with a smooth transition.

There are several criteria that need to be met before a mesh can be considered acceptable for CFD study, including initial cell height, growth ratio, and ultimate layer height. The user has additionally to examine the mesh quality metrics as well as the overall level of resolution in locations of interest. These requirements differ from case to case and necessitate an examination on a case-by-case basis. Table 1 exhibits the details for the mesh grid. It is noteworthy that standard meshing is more suitable for this type of problem.

Boundary conditions

In the solver's setup definition, an absolute frame was used. In fact, since the rotating zone walls were separated from the static zone walls, much of the flow away from the propeller would have a low velocity. The turbulence intensity amounted to 0.1% on the inlet, and slip condition was imposed. It indicates that the fluid adheres to the wall and moves at the same velocity as the wall, if it is moving. This is the case in our study

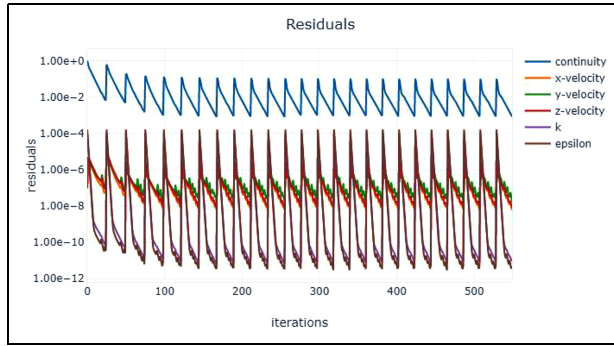


Figure 5. Residual transient state.

because the static zone walls were spaced far enough apart to ensure this condition.

An MRF was assigned to the propeller's rotating domain to account for the rotational movement of the grid cells. MRF simulations required far less computational power than transient modeling. As a result, if the problem is properly set up, MRF can provide good approximations while requiring less computational effort and time. The rotating zone propeller wall was also assigned a rotational designation. Using a Semi-Implicit Method for Pressure-Linked Equations, the pressure-velocity coupling was accomplished. For velocity and pressure, the Second Order Upwind method was applied. The gradients were computed using the Least Square Cell-based Algorithm as well as the second Order Upwind for Turbulent Kinetic Energy and Turbulent Dissipation Rate.

The two-equation models k - ϵ and k - ω models present a general description of turbulence through two transport equations. One for the turbulence kinetic energy k and the other for the specific turbulence dissipation rate ω . They all rely on Boussinesq's approximation from 1877, where the stress tensor is modeled in the viscous term of Navier-Stokes Equation. As far as our simulation is concerned, the standard k - ϵ model, requiring a fully turbulent flow, was used to simulate turbulence. The convergence was also ensured through monitoring the residual value as it falls below a certain threshold. This would be an indicator of a mathematical solution implying that the simulation was able to stabilize. However this means on the other side only a mathematical convergence, as monitoring physical parameters such as force, drag, or average temperature might help the users determine whether their study yielded a feasible solution.⁴⁹

Results and discussions

The force and momentum of a propeller were resolved in a three-coordinate system with the parameters x , y , and z , where T (N) is thrust, Q (N m) is torque, n (rps)

| | Value | Absolute Criteria | Convergence Status |
|------------|--------------|-------------------|--------------------|
| continuity | 0.0008600885 | 0.001 | Converged |
| epsilon | 4.861372e-12 | 0.001 | Converged |
| k | 9.260715e-12 | 0.001 | Converged |
| x-velocity | 6.044336e-09 | 0.001 | Converged |
| y-velocity | 1.819587e-08 | 0.001 | Converged |
| z-velocity | 7.709716e-09 | 0.001 | Converged |

Figure 6. Status of convergence for the residuals.

is propeller rotational speed per second, d (m) is diameter, and ρ is fluid density. Both the thrust coefficient, C_T , and the torque coefficient, C_Q , have a relative percentage error. The numerical analysis results were compared to available experimental data so as to confirm the grid's influence.¹

$$\Delta = \frac{C_{TCFD} - C_{TEXP}}{C_{TEXP}} * 100 \quad (9)$$

$$C_T = \frac{T}{\rho n^2 D^4} \quad (10)$$

Results

In the solution method task page, the SIMPLE resolution method uses a relationship between velocity and pressure corrections to ensure mass conservation and to obtain the pressure field. In addition, for the transient algorithm, a second order implicit formulation was used. Second order algorithms entail the greatest results since they decrease interpolation mistakes significantly. Furthermore, the simulation was then initiated with 1e-006-time steps and 100 iterations by time step. In this approach, higher-order accuracy was achieved at cell faces through a Taylor series expansion of the cell-centered solution about the cell centroid, with a slower convergence.

In a CFD analysis, the residual measures the local imbalance of a conserved variable in each control volume. Every cell in your model is assigned its own residual value for each of the equations being solved.

For CFD, RMS residual levels of 1E-4 are considered loosely converged, while 1-5 is regarded well converged and 1-6 is considered tightly converged. Figure 5 illustrates a screen shot from the Ansys fluent report, Figure 6 shows the status of convergence for all the residuals.

For complicated problems, however, it's not always possible to achieve residual levels as low as 1E-6 for a simple problem. In our simulation, the achieved residuals are as low as 1E-6.

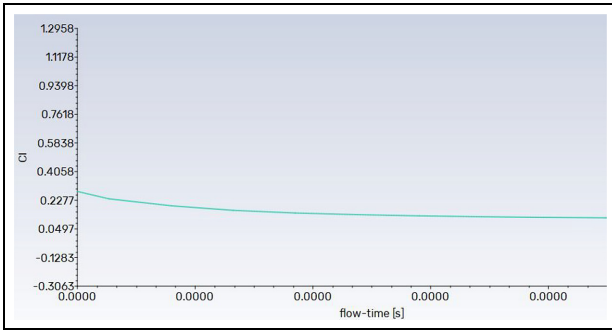


Figure 7. Solution convergence.

Table 2. CT from cfd and CT from experiments.

| Speed | CT cfd | CT exp |
|-------|--------|--------|
| 2500 | 0.1041 | 0.1039 |
| 3000 | 0.091 | 0.1100 |
| 3500 | 0.0915 | 0.1117 |
| 4000 | 0.0914 | 0.1158 |
| 4500 | 0.094 | 0.12 |
| 5000 | 0.096 | 0.1237 |

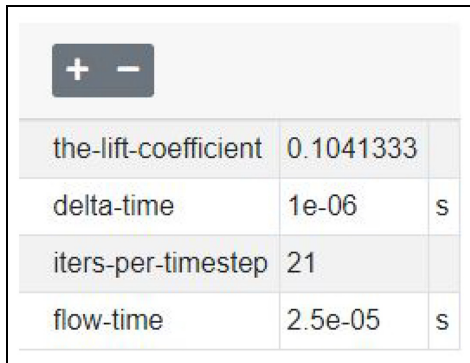


Figure 8. Static thrust coefficient for 2500 RPM.

For an analysis to be called converged, the solution field should not fluctuate from an iteration to an iteration. In our board design, the drag and the lift can be invested as monitor points in the experimental as well as in the simulation studies. In our case, the lift coefficient was chosen as the physical monitor. The corresponding solution yields stable progression of results when changing RPM. The pattern of the thrust coefficient was stabilized with minimum computational cost, as shown in Figure 7.

The experimental data from data source created by the University of Illinois at Urbana-Champaign were used to assess the results found by the CFD analysis. As provided in Table 2 and Figure 8, the first simulation was conducted for 2500 RPM speed. The result provided in the ansys fluent is outlined in Figure 8.

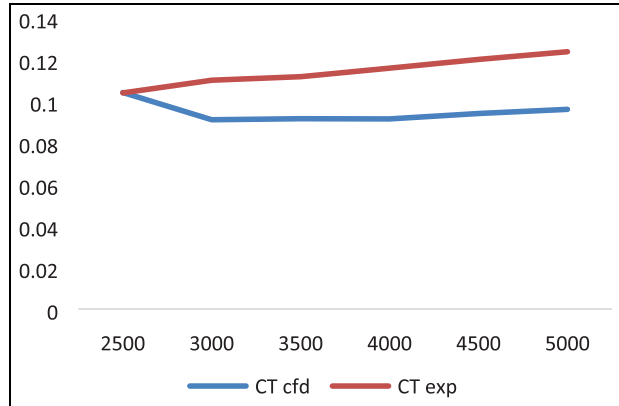


Figure 9. Comparison from CT from cfd and CT from experiments.

Table 3. Thrust coefficient from conventional propeller and curved tip propeller for static performance.

| Speed | Conventional propeller CT | Curved tip propeller CT |
|-------|---------------------------|-------------------------|
| 2500 | 0.1039 | 0.1237 |
| 3000 | 0.1100 | 0.1372 |
| 3500 | 0.1117 | 0.1398 |
| 4000 | 0.1158 | 0.1375 |
| 4500 | 0.12 | 0.1568 |
| 5000 | 0.1237 | 0.1623 |

The now-selected model was copied, and the propeller's shape was modified using Solidworks 2020 to bind the tips. Our major target lies in designing curved tips that mimic the intersection of the propeller and the commonly used duct in these situations. After bending the tips in Solidworks, we proceeded with a geometry correction using the ansys space claim tool to eliminate miscreated corners, fuse surfaces, and point out the problematic geometries, after which the modified propeller will be injected in the duplicated model by simply replacing the old one. The meshing sizing was also determined using the same method as the previous simulation and retaining the same meshing parameters. Table 3 and Figure 9 as well as Figure 10 illustrate the CT difference between conventional type and curved type propeller.

At this stage of analysis, using an advance ratio J to simulate the flying state by imposing an air speed in the inlet from j is indicated by the formula $J = \frac{V}{n*D}$. The results suggest that the curved-tip propeller has a better thrust for the vast majority of j .

A key parameter of interest is the thrust coefficient (Ct), which encapsulates the efficiency of the propeller design. The drone's flight time (T) and its payload carrying capacity are critically dependent on this coefficient they are calculated by coupling ansys fluent results

Table 4. Effect of thrust coefficient on flight time and payload capacity: a comparison between conventional and curved tip propellers.

| J | CT_conventional tip | CT_curved_tip | Flight time modified | Flight time conventional | Max payload curved tip | Max payload conventional tip |
|-----------------|---------------------|---------------|----------------------|--------------------------|------------------------|------------------------------|
| 4000 RPM | | | | | | |
| 0.1 | 0.0994 | 0.1106 | 0.814 | 0.905 | 430.662 | 386.747 |
| 0.2 | 0.0944 | 0.1062 | 0.847 | 0.953 | 413.410 | 367.142 |
| 0.2 | 0.0885 | 0.1035 | 0.869 | 1.017 | 402.823 | 344.008 |
| 0.3 | 0.0829 | 0.0917 | 0.981 | 1.086 | 356.555 | 322.050 |
| 0.3 | 0.077 | 0.0874 | 1.03 | 1.169 | 339.695 | 298.916 |
| 0.3 | 0.0719 | 0.0785 | 1.146 | 1.252 | 304.798 | 278.919 |
| 0.4 | 0.0652 | 0.0753 | 1.195 | 1.380 | 292.251 | 252.649 |
| 0.4 | 0.0582 | 0.0637 | 1.413 | 1.546 | 246.767 | 225.202 |
| 0.4 | 0.0502 | 0.0565 | 1.593 | 1.793 | 218.536 | 193.834 |
| 0.5 | 0.0441 | 0.0506 | 1.779 | 2.041 | 195.402 | 169.916 |
| 0.5 | 0.0343 | 0.0401 | 2.245 | 2.624 | 154.232 | 131.490 |
| 0.5 | 0.0288 | 0.0339 | 2.655 | 3.126 | 129.921 | 109.924 |
| 0.6 | 0.0178 | 0.0201 | 4.479 | 5.058 | 75.8120 | 66.793 |
| 0.6 | 0.0083 | 0.0089 | 10.116 | 10.84 | 31.896 | 29.544 |
| 5000 RPM | | | | | | |
| 0.1 | 0.1077 | 0.1225 | 0.734 | 0.835 | 477.322 | 419.291 |
| 0.1 | 0.1038 | 0.1209 | 0.744 | 0.867 | 471.048 | 404 |
| 0.2 | 0.0993 | 0.1161 | 0.775 | 0.906 | 452.227 | 386.355 |
| 0.2 | 0.0953 | 0.112 | 0.803 | 0.944 | 436.151 | 370.67 |
| 0.2 | 0.0908 | 0.0988 | 0.911 | 0.991 | 384.394 | 353.026 |
| 0.3 | 0.0856 | 0.0961 | 0.936 | 1.051 | 373.808 | 332.637 |
| 0.3 | 0.0811 | 0.0896 | 1.004 | 1.110 | 348.321 | 315 |
| 0.3 | 0.0766 | 0.0894 | 1.007 | 1.175 | 347.537 | 297.348 |
| 0.4 | 0.0709 | 0.0799 | 1.126 | 1.269 | 310.287 | 275 |
| 0.4 | 0.066 | 0.0708 | 1.271 | 1.364 | 274.606 | 255.785 |
| 0.4 | 0.0597 | 0.0656 | 1.372 | 1.508 | 254.217 | 231.083 |
| 0.4 | 0.0549 | 0.0608 | 1.480 | 1.639 | 235.396 | 212.262 |
| 0.5 | 0.0486 | 0.0532 | 1.692 | 1.852 | 205.597 | 187.560 |
| 0.5 | 0.0428 | 0.0468 | 1.923 | 2.103 | 180.50 | 164.818 |
| 0.5 | 0.0352 | 0.0413 | 2.180 | 2.557 | 158.937 | 135.011 |
| 0.6 | 0.028 | 0.032 | 2.813 | 3.215 | 122.471 | 106.787 |
| 0.6 | 0.0206 | 0.0234 | 3.847 | 4.370 | 88.751 | 77.68 |
| 6000 RPM | | | | | | |
| 0.1 | 0.1171 | 0.1317 | 0.683 | 0.768 | 513.395 | 456.148 |
| 0.12 | 0.1133 | 0.1239 | 0.726 | 0.794 | 482.811 | 441.249 |
| 0.15 | 0.1087 | 0.127 | 0.708 | 0.828 | 494.966 | 423.212 |
| 0.17 | 0.1048 | 0.1145 | 0.7863 | 0.859 | 445.954 | 407.920 |
| 0.19 | 0.1009 | 0.1175 | 0.766 | 0.892 | 457.717 | 392.628 |
| 0.22 | 0.0965 | 0.1053 | 0.855 | 0.933 | 409.881 | 375.376 |
| 0.24 | 0.0932 | 0.1093 | 0.823 | 0.966 | 425.565 | 362.437 |
| 0.27 | 0.0884 | 0.0977 | 0.921 | 1.018 | 380.081 | 343.616 |
| 0.29 | 0.0847 | 0.0919 | 0.097 | 1.062 | 357.337 | 329.108 |
| 0.32 | 0.0805 | 0.0879 | 1.024 | 1.118 | 341.655 | 312.640 |
| 0.33 | 0.0773 | 0.0881 | 1.021 | 1.164 | 342.440 | 300.093 |
| 0.36 | 0.0728 | 0.0816 | 1.103 | 1.236 | 316.953 | 282.448 |
| 0.38 | 0.0685 | 0.0757 | 1.189 | 1.314 | 293.819 | 265.588 |
| 0.41 | 0.0629 | 0.0734 | 1.226 | 1.431 | 284.801 | 243.630 |
| 0.43 | 0.0581 | 0.0659 | 1.366 | 1.549 | 255.393 | 224.810 |
| 0.45 | 0.0532 | 0.0601 | 1.490 | 1.692 | 232.652 | 205.597 |
| 0.48 | 0.048 | 0.0565 | 1.593 | 1.875 | 218.536 | 185.207 |

to a developed MATLAB algorithm results are illustrated in Table 4 and represented with Figure 11 for

4000 RPM, Figure 12 for 5000 RPM, and Figure 13 for 6000 RPM.

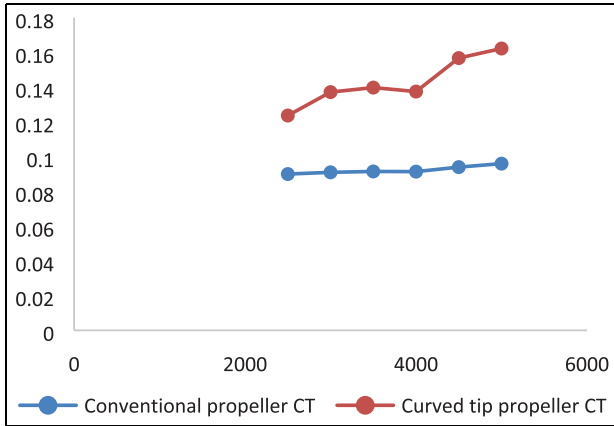


Figure 10. Comparison between thrust coefficient from conventional and curved tip propeller.

Discussions

Using the data summarized in Table 4, our analysis compared conventional and curved propellers, where the curved propeller exhibited a 15.9% higher average Ct and 6.1% greater maximum payload capacity. However, the flight time for drones with curved

propellers was approximately 6.7% lower than for those with conventional propellers. Indeed, the relationship between thrust coefficient and thrust is represented by equation (10).

Referring to the prevalence of Li-Po cells and batteries in commercial UAVs, they were utilized for these computations. The energy consumption calculation was largely based on the information cited in the bibliography for the vertical upward energy consumption.^{50,51} The amount of energy used from the battery grows as the time of takeoff for flights at higher altitudes increases.

The formula that links the thrust and the weight is determined as⁵²

$$F_{t,v} = M_{tot}g + \frac{1}{2}\rho A_t C_d V_v^2 = M_{tot} g + \frac{1}{2}\rho A_t C_d V_v^2 \quad (11)$$

For this mission profile, the drone will be hovering for most of the flight. Therefore, we may disregard the vertical speed V_v^2 . The thrust is hence a function of mass alone, and the gain is transferred to the overall weight of the payload. Notably, the increase in thrust will need additional power to be supplied, as thrust and power are closely connected by this equation⁵³

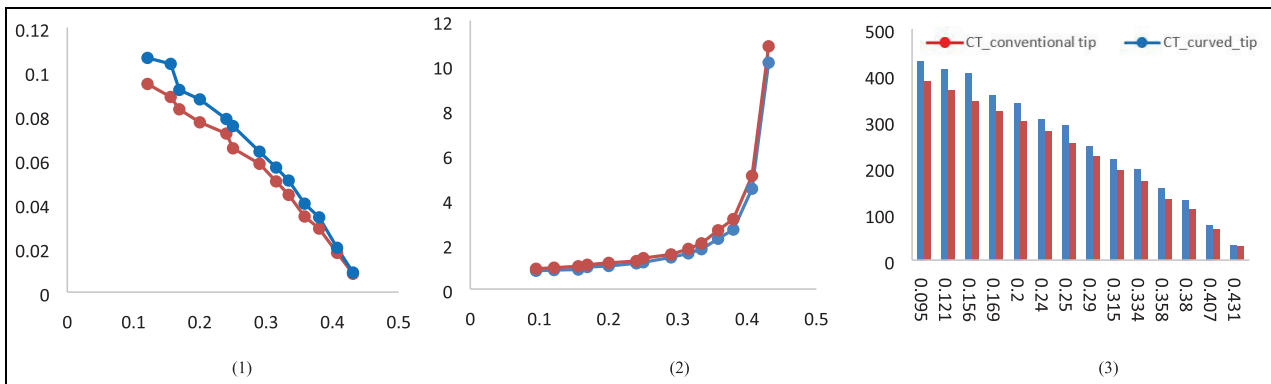


Figure 11. Comparison between curved tip propeller and conventional tip propeller for 4000 RPM: 1 – thrust coefficient, 2 – flight time duration, 3 – maximum payload.

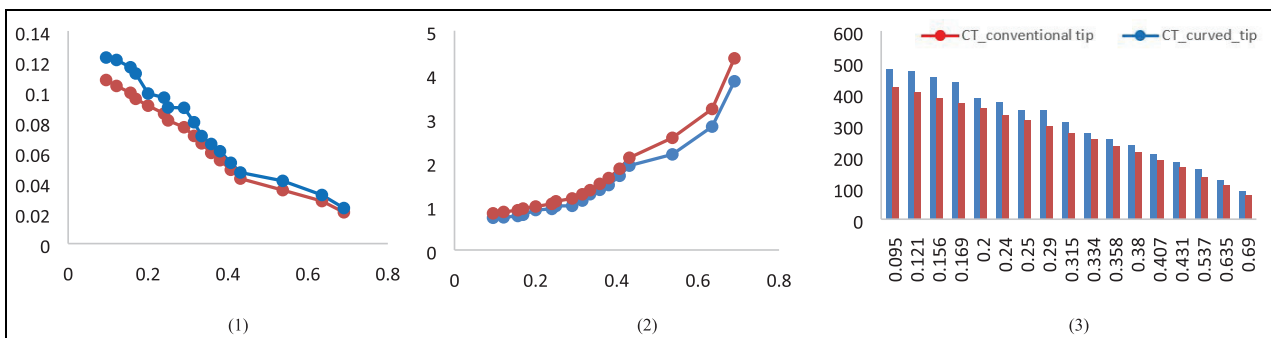


Figure 12. Comparison between curved tip propeller and conventional tip propeller for 5000 RPM: 1 – thrust coefficient, 2 – flight time duration, 3 – maximum payload.

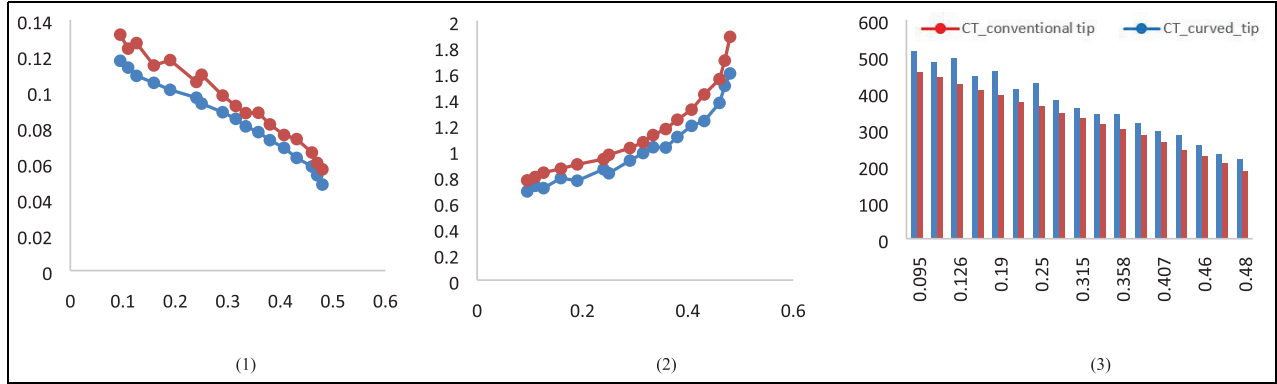


Figure 13. Comparison between curved tip propeller and conventional tip propeller for 6000 RPM: 1 – thrust coefficient, 2 – flight time duration, 3 – maximum payload.

$$P = \sqrt{\frac{F^3}{2\rho A_p}} \quad (12)$$

This increase is automatically indicative of an increase in the average amperage draw specified by:

$$AAD = AUW * P/V$$

In our case study, the needed power with the new topology was multiplied by 14. Thus, if we chose to install this modified propeller with the same batteries, we would have a time of flight^{47,53} expressed by equation (13):

$$T' = \text{capacity} \times \text{discharge} / AAD' \quad (13)$$

$$T' = \text{capacity} \times \text{discharge} / [(AUW * P')/V]$$

The results emphasize the trade-off between thrust coefficient, flight time, and payload capacity, highlighting the need for optimizing propeller design for lift generation and energy efficiency. The most promising aspect of this type of propellers is their potential to accommodate greater payloads while maintaining the same size. Future research should focus on advanced propeller shapes and materials to achieve a balance between these factors.

Conclusion

This study presents a simulation of an altered propeller shape using a CFD model developed on ANSYS fluent to investigate its performance. The choice of the propeller type is based on a SCILLAB simulation presented in Chakchouk et al.⁴⁷ As for the verification and validation of the CFD model, we invested the APC propeller data set developed by University of Illinois at Urbana-Champaign. The convergence study of the solution was monitored both mathematically and physically, opting for the thrust coefficient as the main monitor.

This study is, to the best of our knowledge, the pioneer investigation of a curved tip propeller employed on a drone addressing its merits and deficiencies on the mission profile. The computational trend under static or forward flying conditions over the whole range of advance ratios (j) values indicated the performance advantage that may be achieved employing curved tip propellers. Results revealed that an estimated 25% increase in thrust force can be reached, which translates a capability for hovering to lift a load heavier than the initial load intended with the selection of the same propeller when it is conventional, yielding a more capable propeller with the same dimensions. However, the increase of thrust has a negative impact on the drone's flying duration, which was shortened by 30%.

This shortcoming can be mitigated by cooperative task assignment of multi-UAV system. Besides, future study will explore the optimization of the other components of the system, such as the drone chassis and landing gear, motivated by the promising characteristics of this topology.


Declaration of conflicting interests

The author(s) declared no potential conflicts of interest with respect to the research, authorship, and/or publication of this article.

Funding

The author(s) disclosed receipt of the following financial support for the research, authorship, and/or publication of this article: This work was done in a collaboration between the LMN laboratory of INSA Rouen Normandie and the LATMOS laboratory of the University of Versailles St-Quentin Paris-Saclay, in support by LA2MP laboratory of Sfax and we thank all of these institutions for support. Fruitful discussions with Doctor Hichame Maaname are greatly acknowledged.

ORCID iD

Mohamed Abdessamia Chakchouk  <https://orcid.org/0009-0004-1415-9888>

References

1. Bergmann D, Denzel J, Pfeifle O, et al. In-flight lift and drag estimation of an unmanned propeller-driven aircraft. *Aerospace* 2021; 8: 43.
2. Wald QR. The aerodynamics of propellers. *Prog Aerosp Sci* 2006; 42: 85–128.
3. Jiang H, Wu H, Chen W, et al. Toward high-efficiency low-noise propellers: a numerical and experimental study. *Phys Fluids* 2022; 34: 076116.
4. Yang Y, Veldhuis LLM and Eitelberg G. Aerodynamic impact of a streamwise vortex on a propeller. *Aerosp Sci Technol* 2017; 70: 108–120.
5. Okulov VL, Sørensen JN and Wood DH. The rotor theories by Professor Joukowski: vortex theories. *Prog Aerosp Sci* 2015; 73: 19–46.
6. Rostami M and Farajollahi AH. Aerodynamic performance of mutual interaction tandem propellers with ducted UAV. *Aerosp Sci Technol* 2021; 108: 106399.
7. Mi BG. Numerical investigation on aerodynamic performance of a ducted fan under interferences from the ground, static water and dynamic waves. *Aerosp Sci Technol* 2020; 100: 105821.
8. Han H, Xiang C, Xu B, et al. Aerodynamic performance and analysis of a hovering micro-scale shrouded rotor in confined environment. *Adv Mech Eng* 2019; 11: 1687814018823327.
9. Graduate AA, Assistant R and Camci C. Double Ducted Fan (DDF) as a novel ducted fan inlet lip separation control device. *Presented at the International powered lift conference, 5–7 October 2010, Philadelphia, PA, USA, 2010.*
10. Akturk A and Camci C. Experimental and computational assessment of a ducted-fan rotor flow model. *J Aircr* 2012; 49: 885–897.
11. Chen J, Li L, Huang G, et al. Numerical investigations of ducted fan aerodynamic performance with tip-jet. *Aerosp Sci Technol* 2018; 78: 510–521.
12. Hu Y, Qing JX, Liu ZH, et al. Hovering efficiency optimization of the ducted propeller with weight penalty taken into account. *Aerosp Sci Technol* 2021; 117: 106937.
13. ElGhazali AF and Dol SS. Aerodynamic optimization of unmanned aerial vehicle through propeller improvements. *J Appl Fluid Mech* 2020; 13: 793–803.
14. Liu Y, Tan L and Wang B. A review of tip clearance in propeller, pump and turbine. *Energies* 2018; 11: 2202.
15. Tran BN, Jeong H, Kim JH, et al. Effects of tip clearance size on energy performance and pressure fluctuation of a tidal propeller turbine. *Energies (Basel)* 2020; 13: 4055.
16. Liu Y and Tan L. Influence of C groove on suppressing vortex and cavitation for a NACA0009 hydrofoil with tip clearance in tidal energy. *Renew Energy* 2020; 148: 907–922.
17. Andichamy Gohar VC, Khokhar T and Camci C. An experimental study of using vortex generators as tip leakage flow interrupters in an axial flow turbine stage. In: *ASME Turbo Expo 2018: turbomachinery technical conference and exposition*, Oslo, Norway, 11–15 June 2018.
18. Shi L, Zhang D, Zhao R, et al. Effect of blade tip geometry on tip leakage vortex dynamics and cavitation pattern in axial-flow pump. *Sci China Technol Sci* 2017; 60: 1480–1493.
19. Han Y and Tan L. Influence of rotating speed on tip leakage vortex in a mixed flow pump as turbine at pump mode. *Renew Energy* 2020; 162: 144–150.
20. Adeyeye KA, Ijumba N and Colton J. The effect of the number of blades on the efficiency of a wind turbine. *IOP Conf Ser Earth Environ Sci* 2021; 801: 012020.
21. Jiang Y and Zhang B. Numerical investigation of effect of parameters on hovering efficiency of an annular lift fan aircraft. *Aerospace* 2016; 3: 35.
22. Homa M, Pałac A, Żołądek M, et al. Small-scale hybrid and polygeneration renewable energy systems: energy generation and storage technologies, applications, and analysis methodology. *Energies* 2022; 15: 9152.
23. Lazaro Echavarria CM and Poroseva SV. Computational analysis of the blade number effect on the performance of a ducted propeller. In: *AIAA atmospheric flight mechanics conference*, Kissimmee, FL, USA, 5–9 January 2015.
24. Hrishikeshavan V, Black J and Chopra I. Design and testing of a quad shrouded rotor micro air vehicle in hover. In: *53rd AIAA/ASME/ASCE/AHS/ASC structures, structural dynamics and materials conference*, Honolulu, HI, USA, 23–26 April 2012.
25. Roberts WB, Armin A, Kassaseya G, et al. The effect of variable chord length on transonic axial rotor performance. *J Turbomach* 2002; 124: 351–357.
26. Wisniewski CF, Byerley AR, Heiser WH, et al. The influence of airfoil shape, tip geometry, Reynolds number and chord length on small propeller performance and noise. In: *33rd AIAA applied aerodynamics conference*, Dallas, TX, USA, 22–26 June 2015.
27. Zhang T, Qiao G, Smith DA, et al. Parametric study of aerodynamic performance of equivalent ducted/unducted rotors. *Aerosp Sci Technol* 2021; 117: 106984.
28. Fan C, Amankwa Adjei R, Wu Y, et al. Parametric study on the aerodynamic performance of a ducted-fan rotor using free-form method. *Aerosp Sci Technol* 2020; 101: 105842.
29. Guerrero J, Sanguinetti M and Wittkowski K. CFD study of the impact of variable cant angle winglets on total drag reduction. *Aerospace* 2018; 5: 126.
30. Makgantai B, Subaschandar N and Jamisola RS. A review on wingtip devices for reducing induced drag on fixed-wing drones. *J Xi'an Univ Archit Technol* 2021; 13: 143–160.
31. Cerón-Muñoz HD and Catalano FM. Experimental analysis of the aerodynamic characteristics adaptive of multi-winglets. *Proc IMechE, Part G: J Aerospace Engineering* 2006; 220: 209–215.
32. Sweetly M, Samuel G, Manikandan G, et al. Design and performance analysis of spiroid winglet with normal wing aircraft. *Imp J Interdiscip Res* 2017; 3: 773–778.

33. Raj WG and Thomas TA. Design and analysis of spiroid winglet. *Int J Innov Res Sci Eng Technol* 2007; 4: 1139–1147.
34. Samal SK and Dash PK. Reduction of wingtip vortices by using active means. *Int J Sci Eng Res* 2013; 4: 1280–1287.
35. Yilmaz E and Hu J. Cfd study of quadcopter aerodynamics at static thrust conditions. In: *Proceedings of the ASEE Northeast 2018 annual conference*, West Hartford, CT, USA, 2018. pp. 27–28.
36. Brandt JB and Selig MS. Propeller performance data at low reynolds numbers. In: *49th AIAA aerospace sciences meeting including the new horizons forum and aerospace exposition*, 2011. p. 1255.
37. Giljarhus KET, Porcarelli A and Apeland J. Investigation of rotor efficiency with varying rotor pitch angle for a coaxial drone. *Drones* 2022; 6: 91.
38. Bontempo R, Cardone M, Manna M, et al. Ducted propeller flow analysis by means of a generalized actuator disk model. *Energy Proc* 2014; 45: 1107–1115.
39. Gaggero S and Ferrando M. Wake instabilities of tip-loaded propellers: comparison between CLT and ‘New Generation’ CLT configurations. *J Mar Sci Eng* 2023; 11: 112.
40. Shin KW and Andersen P. CFD analysis of cloud cavitation on three tip-modified propellers with systematically varied tip geometry. *J Phys Conf Ser* 2015; 656: 012139.
41. Inukai Y. A development of a propeller with backward tip raked fin. In: *Third international symposium on marine propulsion, smp’13*, TAS, Australia, May 2013.
42. Shin KW and Andersen P. CFD analysis of scale effects on conventional and tip-modified propellers. In: *Fifth international symposium on marine propulsors, smp’17*, Espoo, Finland, June 2017.
43. Cheng HJ, Chien YC, Hsin CY, et al. A numerical comparison of end-plate effect propellers and conventional propellers. *J Hydrodynam* 2010; 22: 478–483.
44. Chekab MAF, Ghadimi P, Reza Djeddi S, et al. Investigation of different methods of noise reduction for submerged marine propellers and their classification. *Am J Mech Eng* 2013; 1: 34–42.
45. Andersen P, Kappel JJ, Spangenberg E, et al. Aspects of propeller developments for a submarine. In: *First international symposium on marine propulsors, smp’09*, Trondheim, Norway, June 2009.
46. Chakchouk MA, El Hami A and Haddar M. La fiabilité appliquée à la conception du dispositifs spectromètre mobile I; optimisation des paramètres de vols. 2022.
47. Chakchouk MA, el Hami A, Gafsi W, et al. Design discussion of a mobile and intelligent infrared detector for the measurement of the air quality index. In: Ben Amar M, Bouguecha A, Ghorbel E, et al. (eds) *Advances in materials, mechanics and manufacturing II*. Cham: Springer, 2022, pp.342–352.
48. Vargas Loureiro E, Oliveira NL, Hallak PH, et al. Evaluation of low fidelity and CFD methods for the aerodynamic performance of a small propeller. *Aerosp Sci Technol* 2021; 108: 106402.
49. Versteeg HK and Malalasekera W. *An introduction to computational fluid dynamics*. 2nd ed. Harlow: Pearson Education Ltd, 2007.
50. Prasetia AS, Wai RJ, Wen YL, et al. Mission-based energy consumption prediction of multirotor UAV. *IEEE Access* 2019; 7: 33055–33063.
51. Hwang MH, Cha HR and Jung SY. Practical endurance estimation for minimizing energy consumption of multirotor unmanned aerial vehicles. *Energies (Basel)* 2018; 11: 2221.
52. Chen Y, Baek D, Bocca A, et al. A case for a battery-aware model of drone energy consumption. In: *2018 IEEE international telecommunications energy conference (INTELEC)*, Turino, Italy, 7–11 October 2018.
53. Kim J, Kim S, Jeong J, et al. CBDN: cloud-based drone navigation for efficient battery charging in drone networks. *IEEE Trans Intell Transp Syst* 2019; 20: 4174–4191.

Appendix

List of symbols, acronyms, and abbreviations

| | |
|--------|---------------------------------|
| FTIR | Fourier Transform Infrared |
| CFD | Computational Fluid Dynamics |
| APC | Advanced Precision Composites |
| UAV | Unmanned Aerial Vehicle |
| SCILAB | Scientific Laboratory |
| RPM | Revolutions Per Minute |
| ANSYS | Analysis Systems |
| CAD | Computer-Aided Design |
| RANS | Reynolds-Averaged Navier-Stokes |
| MRF | Multiple Reference Frame |
| RMS | Root Mean Square |
| CD | Coefficient of Drag |
| Ct | Coefficient of thrust |
| Li-Po | Lithium Polymer |
| AUW | All-Up Weight |
| V | Voltage |
| AAD | Average Amperage Draw |